EFFECT OF STRUCTURAL ORDERING OF THE CARBON SUPPORT ON THE BEHAVIOR OF Pd CATALYSTS IN AQUEOUS-PHASE HYDRODECHLORINATION

José A. Baeza[1], Luisa Calvo[1], Noelia Alonso-Morales[1], Francisco Heras[1], Semih Eser[2], Juan J. Rodriguez[1], Miguel A. Gilarranz[1]

[1]*S.D. Ingeniería Química, Universidad Autónoma de Madrid, Av/ Francisco Tomás y Valiente 7, 28049 Madrid, Spain*

[2]*John and Willie Leone Family Department of Energy and Mineral Engineering and EMS Energy Institute, The Pennsylvania State University, 114A Hosler Building, University Park, PA 16802, United States*

Abstract

Catalysts consisting of Pd supported on virgin and heat-treated carbon blacks (homemade and commercial), graphites (natural and synthetic) and commercial carbon nanofibers were prepared and tested in the aqueous phase hydrodechlorinaton (HDC) of 4-chlorophenol (4-CP) under near ambient conditions (30 ºC, 1 atm) in order to explore the effect of the support on the catalytic behavior. The homemade graphitized supports were prepared from commercial carbon black (CB) and from a carbon black-like material (CBPE) obtained from pyrolysis of low-density polyethylene. All the catalysts prepared yielded complete 4-CP conversion, although a wide range of activity was observed (10.7 – 173.5 $mmol \cdot g_{Pd}^{-1} \cdot min^{-1}$). The graphitized carbon black provided the most active catalysts, showing Pd nanoparticles around 3 nm in size and a well-balanced contribution of Pd species (Pd^{n+}/Pd^0 = 0.9). Substantial

differences of activity were found between the graphitized and not graphitized supports, even for catalysts with similar Pd nanoparticle size. The higher activity of the catalysts with graphitized supports can be partly associated to a more balanced initial Pd^{n+} to Pd^{0} ratio. Moreover, higher selectivity to hydrogenation products (cyclohexanone) was also achieved with those catalysts due to a higher contribution of the Pd^{0} species.

Keywords: Graphitized support, carbon black, hydrodechlorination, 4-chlorophenol

1. Introduction

In the last few years the economic impact of catalysis has been increasing, since the world's demand for catalysts is growing at almost 6 % per year [1]. The relevance of catalysis in the chemical industry is outstanding, taking into account that 85-90 % of chemical products needs of a catalyst during their production [2]. Among all the catalytic processes used in the industry, heterogeneous catalysis is by far predominant (80 % of the global catalysts market share), compared to homogeneous (17 %) and enzymatic (3 %) [3]. In heterogeneous catalysis, several materials are used as catalysts supports such as carbon materials, alumina, silica, ceria, zirconia and clays, among others. Carbon materials generate especial interest, being among their main advantages an easily tailorable porous structure and surface chemistry, high resistance to acids and bases, structure stability at high temperatures under inert atmosphere, simple recovery and comparatively low cost in general [4].

In spite of its availability, graphitic carbons have been much less used than other carbon materials in catalysis due to their low specific surface area (10 - 50 $m^2 \cdot g^{-1}$) and poorly developed pore structure [4]. Nevertheless, graphites have shown fairly good

performance as catalysts supports in different reactions, such as the hydrogenation of citral, where higher selectivity towards the unsaturated alcohol was obtained compared to other conventional supports such as alumina, silica or activated carbon [5]. They have been also used in CO electro-oxidation [6], oxidation of alkenes [7], catalytic decomposition of ammonia [8] and even as bare catalyst in the Baeyer-Villiger oxidation of cyclohexanone, improving the activity and selectivity towards lactones [9].

Other related carbon materials, such as graphitized carbon blacks have also been scarcely explored in catalysis for the same reasons as graphite. They have been mostly used in the fuel cell field as catalysts supports, especially in the oxygen reduction reaction, where the catalyst stability was improved due to enhanced resistance to corrosion [10, 11]. Similar results were found in methanol oxidation [12]. In much less extent, they have been used in other reactions such as CO hydrogenation [13].

In the case of HDC, considered as a potential solution to deal with toxic chlorinated organic compounds [14], studies on catalysts behavior with graphitic supports are scarce, and there is no conclusive agreement about the effect of these supports on catalyst behavior. Thus, some authors reported lower activity of Pd/C or Ni/C catalyst based on graphite compared to other supports in the gas-phase HDC of chlorobenzene [15, 16]. On the contrary, in liquid-phase HDC of tetrachloroethylene, Diaz et al. (2011) [17] reported enhanced catalytic activity when graphites, mechanically modified to increase the porous structure and specific surface area (so-called “high surface area graphite”), were used as supports in Pd/C catalysts. Particularly, in aqueous phase HDC, which is a suitable process for the treatment of wastewater containing organochlorinated pollutants [18], there is a lack of knowledge on this issue.

In the current work, Pd catalysts supported on a set of graphitized and non-graphitized carbons were prepared and tested in the aqueous phase HDC of 4-CP to explore the effect of the structural ordering of the carbon support on the catalysts behavior.

2. Experimental

2.1 Preparation of supports and catalysts

Homemade graphitized supports (CB2800 and CBPE2600) were prepared from a commercial carbon black (CB; Alfa Aesar, 100 % acetylene) and from a carbon black-like material obtained from pyrolysis of low-density polyethylene (CBPE), as described elsewhere [19, 20]. Both CB and CBPE supports were heat-treated at temperatures of 2800 and 2600 ^{o}C, respectively, during 30 min under He flow. Synthetic graphite (SynG, Fluka), natural graphite (NatG, Ticonderoga, NY, USA) and commercial graphitized carbon black (CBMeso, Sigma-Aldrich) and carbon nanofibers (CNF, Sigma-Aldrich) were used as received. The catalysts were prepared by wetness impregnation from an aqueous solution of $PdCl_2$ in 0.1 N HCl. All the catalysts were prepared with a Pd loading of 1 % (w). After the impregnation, the solid was dried for 2 h at room temperature and overnight at 60 ^{o}C, then calcined at 200 ^{o}C for 2 h and reduced with H_2 at 100 ^{o}C for 1 h.

2.2 Characterization of supports and catalysts

The supports were characterized by TEM/STEM at 300 kV (FEI, Tecnai F30), elemental analysis (LECO CHNS-932), nitrogen adsorption-desorption at 77 K (Quantachrome Autosorb I), XRD (X'Pert PRO Panalytical, CuKa-radiation, scanning for 2θ = 5-60^{o}, step size 2θ = 0.033^{o}, count time 200 s), RAMAN spectroscopy (WITex CRM200, λ = 514 nm

and NT-MDT Spectra, λ = 532 nm) and pH slurry. The catalysts were characterized by TEM-STEM/EDS at 300 kV (FEI, Tecnai F30). Software 'ImageJ 1.44i' was used for counting and measuring NPs on digital STEM images (> 200 NPs were measured per sample). Surface-area-weighted mean diameters ($d_s = \sum n_i d_i^3 / \sum n_i d_i^2$) and size distribution, characterized by the standard deviation ($\sigma_s = \sqrt{\sum (d_i - d_s)^2 / n}$), were calculated. Likewise, the catalysts were characterized by XPS (Thermo Scientific, mod. K-Alpha, equipped with an Al Kα X-ray excitation source, 1486.68 eV). Spectrograms deconvolution was performed using XPS peak v4.1 software to determine both Pd^{n+} and Pd^0 species. A Shirley background subtraction and mixed Gaussian–Lorentzian by a least-square method curve fitting was used and C 1s peak (284.6 eV) was used as internal standard for binding energies corrections due to sample charging. Doublet separation for Pd 3d was 5.26 eV.

2.3 HDC experiments

HDC runs were carried out in a jacketed glass reactor (30 ^oC, 1 atm) under 50 N $mL \cdot min^{-1}$ H_2 flow rate, during 4 h. Vigorous stirring (600-800 rpm) was used to facilitate H_2 distribution through the liquid phase (150 mL). The initial concentration of 4-CP was 100 $mg \cdot L^{-1}$ and the Pd loading was 2.5$\cdot mg \cdot L^{-1}$. Vent was provided with reflux system and no significant stripping was detected. Different catalyst loads and stirring velocities were checked in preliminary experiments in order to confirm that the process takes place under chemical control. The liquid samples (1 mL) were collected and filtered (PTFE filter, pore size 0.22 μm). High Performance Liquid Chromatography (Varian Prostar, UV-VIS detector) with a C_{18} column as stationary phase and a mixture of acetonitrile and water (1:1, v/v) as mobile phase, was used to analyze 4-CP and

phenol. Cyclohexanone and cyclohexanol were analyzed by GC/FID (GC 3900 Varian) using a 30 m long x 0.25 mm i.d. capillary column (CP-Wax 52 CB, Varian) and N_2 as carrier gas. The quantification of chloride ion was performed by ion chromatography (Metrohm 790 Personal IC). The carbon and chlorine balances matched between 95.3-99.2% and 96.4-99.5%, respectively.

The rate of 4-CP disappearance was calculated from a pseudo-first order equation:

$$(-r_{4-cp}) = \frac{-dC_{4-cp}}{dt} = k_1 \times C_{4-cp} \qquad [1]$$

$$t = 0; \quad C_{4-cp} = C_0$$

In this model the concentration of H_2 is included in the pseudo-first-order rate constant (k_1), since H_2 was in great excess. The catalysts activity was calculated from the k_1 values, the 4-CP initial concentration and the Pd dose used in the experiments, according to equation [2], where C_{Pd} corresponds to Pd concentration ($g \cdot L^{-1}$).

$$a = k_1 \times \frac{C_{0\,4-CP}}{C_{Pd}} \qquad [2]$$

Taking into account that the adsorption of 4-CP on Pd is significantly favored on terraces atoms rather than edges [21], and the varying fraction of edges with NPs size, which in the case of cubo-octahedron-shaped NPs (which is close to pseudo-spherical shape) can be assumed as $1/d_s$ [22], the activity values were calculated per Pd mass unit instead of TOF because of the broad NP size dispersion obtained for some of the samples in the current work.

3. Results and Discussion

3.1 Characterization of supports

Table 1 shows the specific surface area, micropore and mesopore volume, and the pH slurry of the supports used. The supports exhibited low specific surface area (< 76 $m^2 \cdot g^{-1}$), with negligible micropore and low mesopore volume, allowing the comparison of catalysts behavior with low crossed-effect of variables such as the specific surface area or the porous structure, with the exception of CBMeso, which showed a specific surface area and a mesopore volume of 100 $m^2 \cdot g^{-1}$ and 0.25 $cm^3 \cdot g^{-1}$, respectively. The pH slurry of the supports was in the 4.2 to 7.3 range. Nevertheless, most of them were between 6.0 and 7.3, quite close to the pH of water (6.3). This can be ascribed to the low specific surface of the supports that allowed a limited amount of surface groups. NatG showed the lower surface pH (4.2) probably due to the relatively high amount of S in its surface (0.3%). Table 2 summarizes the elemental composition of the supports. The supports characterized exhibited high C content (> 98.5 %) with the exception of the synthetic and natural graphites due to ash content. The heat-treated carbons CB2800 and CBPE2600 showed higher C and lower H and N contents than CB and CBPE, which can be attributed to the desorption of the H- and N-containing groups at high temperature. The natural graphite (NatG) showed higher H and significantly higher S content compared to the manufactured graphite (SynG).

Table 1. Specific surface area, micropore and mesopore volume, and pH slurry for the supports used.

Support	SSA_{BET} (m^2/g)	Mesopore volume (cm^3/g)	Micropore Volume (cm^3/g)	pH Slurry
CB	76	0.099	<0.001	7.0
CB2800	50	0.003	<0.001	6.5
CBPE	41	<0.001	<0.001	6.2
CBPE2600	<10	<0.001	<0.001	6.2
NatG	<10	<0.001	<0.001	4.2
SynG	<10	<0.001	<0.001	6.2
CNF	24	0.076	<0.001	6.0
CBMeso	100	0.251	<0.001	7.3

Table 2. Elemental composition of the carbon supports used

Support	Elemental composition (w %)			
	C	***H***	**N**	**S**
CB	98.56	0.09	0.05	-
CB2800	98.62	0.02	0.01	-
CBPE	99.19	0.66	0.02	-
CBPE2600	99.96	0.01	0	-
NatG	93.27	0.08	0.01	0.3
SynG	92.50	0.02	0.02	0.03
CNF	98.31	0.01	0.04	0.02
CBMeso	98.78	0.01	0.05	0.02

Figures 1a and b show the TEM and STEM images of selected catalysts and supports. The CBPE and CB supports consist of clusters of carbon spherules. The size of the individual spherules is uniform in each sample, the average diameter being around 750 nm and 50 nm, respectively. These two supports maintain the cluster morphology after heat treatment (CB2800 and CBPE2600). In the case of CB2800, a change from pseudo-globular to polyhedral-like units consisting of graphite sheets surrounding amorphous carbon was observed. In the case of CBPE2600 is appreciable a change

from a smooth and round surface to a faceting one exhibiting polyhedral-like units. These morphological changes are the result of chemical modifications and rearrangement of the graphene layers, leading to a more extensive stacking of them, thus increasing the structural order of the carbon support [23]. SynG and NatG show a graphite microstructure with a higher prevalence of graphite layers. CBMeso showed almost equivalent appearance to CB2800 and CNFs were formed by conical platelets with about 85 nm of diameter and 20-200 µm length. Figure S1 (Supplementary Materials) shows TEM images of Pd/CBMeso and Pd/CNF.

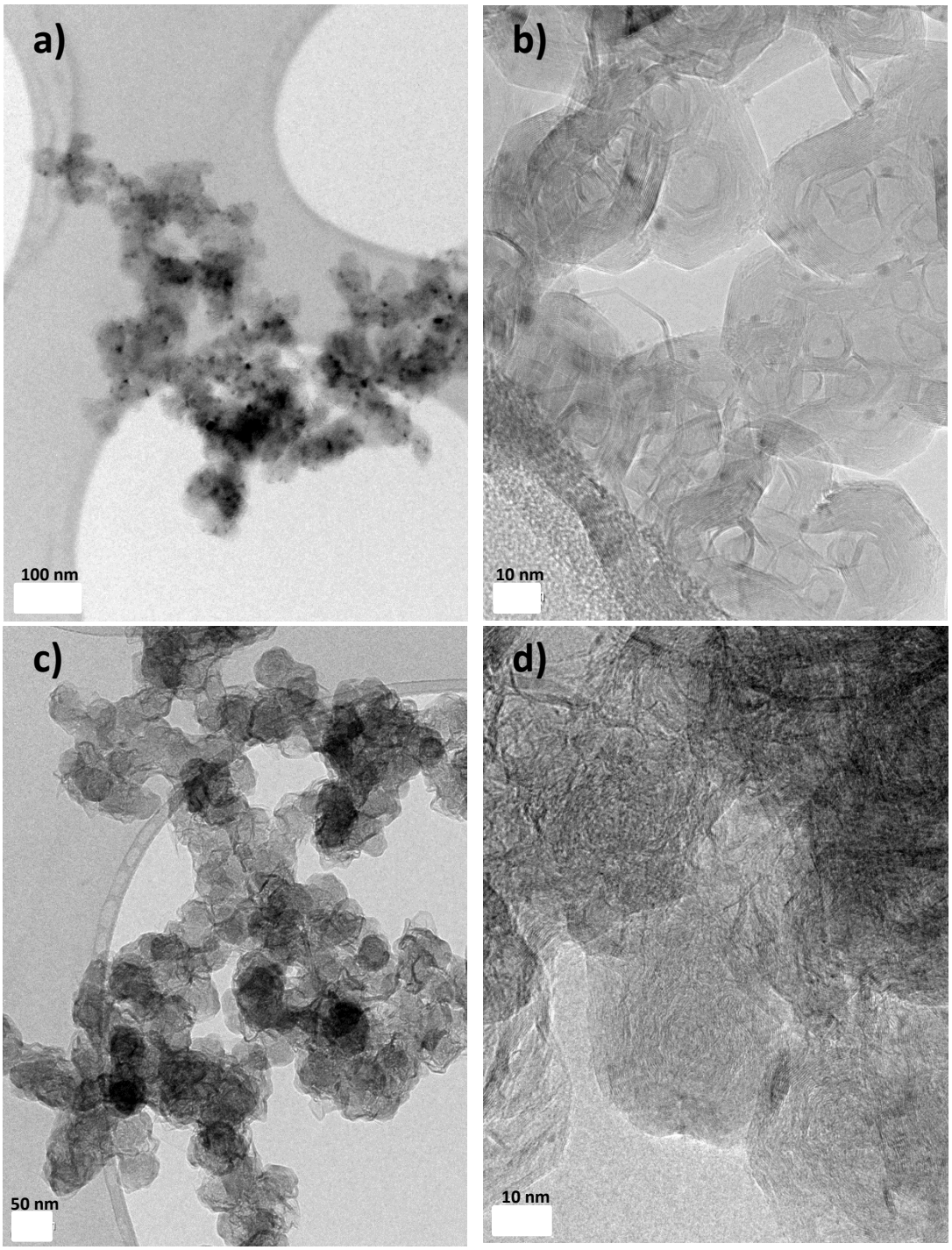

Figure 1a. TEM images of (a, b) Pd/CB2800 and (c, d) Pd/CB.

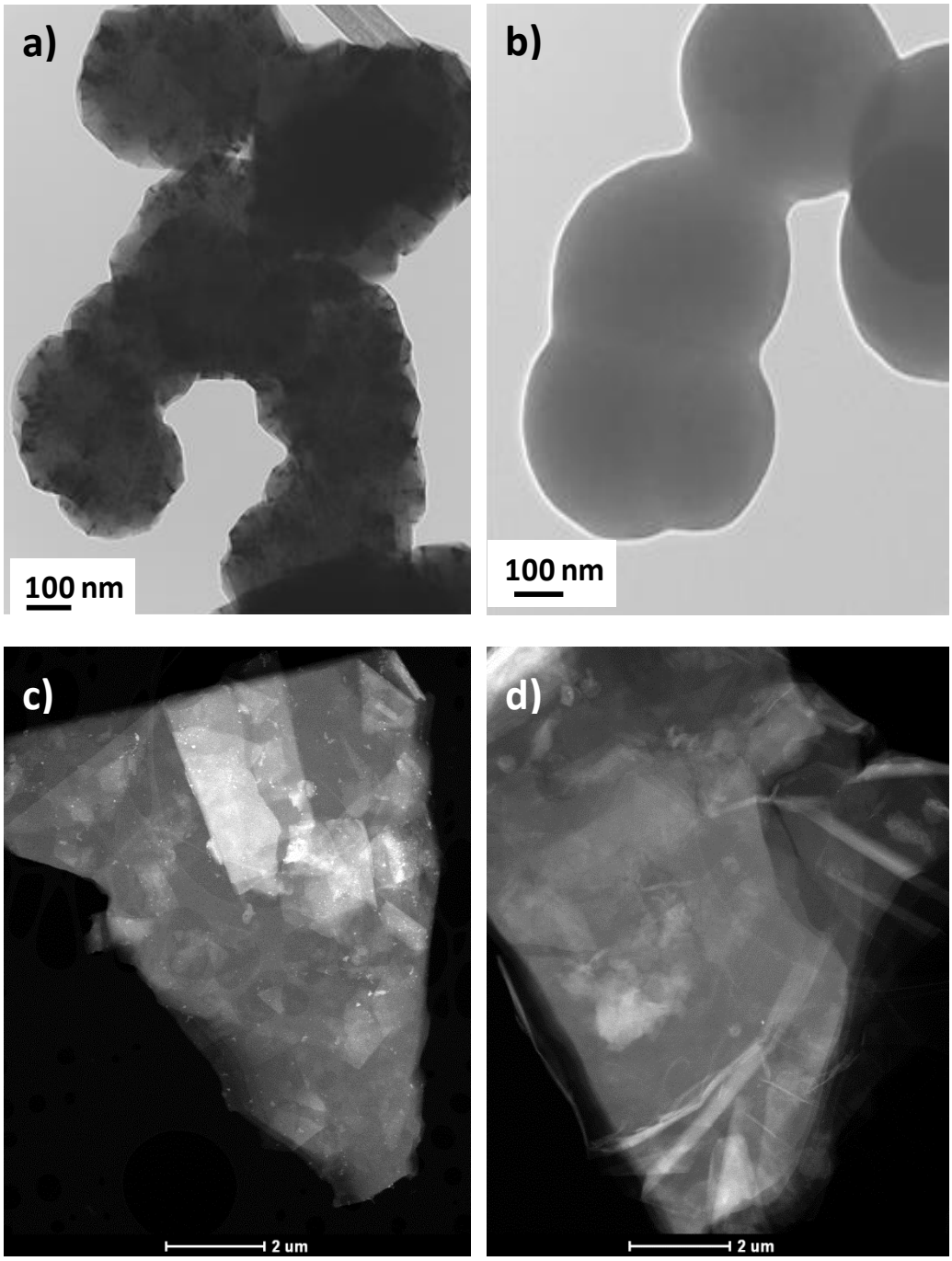

Figure 1b. TEM images of a) CBPE2600, b) CBPE and STEM images of c) Pd/NatG and d) Pd/SynG catalysts.

The carbon supports were analyzed by XRD in order to compare the structural ordering of these materials. Figure 2 shows XRD profiles where the (0 0 2), (1 0 0) and (0 0 4) bands can be observed. The (0 0 2) band becomes more intense and sharper for graphites (SynG and NatG). The (0 0 2) band of CB2800 and CBPE2600 changed considerably with respect to the corresponding carbons before heat treatment (CB and CBPE), indicating a high structural development of the two dimensions ordering upon the heat treatment. This change is mainly ascribed to the removal of volatile species and various defects of the CB and CBPE carbons, which allows the organization of amorphous carbon into graphite layers, leading to the formation and/or the growing of microcrystallites [23, 24]. The (0 0 4) peak which is indicative of the 3D ordering of the graphene layers into the regular sequence of hexagonal graphite [25], appears well defined in samples SynG and NatG, confirming the crystalline structure of these samples.

The values of the crystallite parameters (interplanar spacing, d_{002}, and the crystallographic dimensions, L_c and L_a) of the carbon supports are summarized in Table 3. The graphites showed the highest structural ordering of these carbon supports with values of the interlayer spacing (d_{002}), 0.335 nm, estimated average stacking height (L_c), 385-475 nm and average diameter of crystallites (L_a), 738-1100 nm.

CB and CBPE were the carbon materials with the lowest order, as can be seen from the highest d_{002} values and lowest L_c and L_a dimensions, although CB was slightly more ordered than CBPE. Both CB2800 and CBPE2600 samples increased considerably the structural ordering respect to the starting CB and CBPE carbons. Although CB had a more ordered incipient structure than CBPE, CB2800 developed less crystallinity than CBPE2600 in spite of the higher treatment temperature. This fact can be related to the

morphology of these samples, which are composed by cluster of spherules of fairly different size (750 nm for CBPE and 50 nm for CB). The shape and size of these initial particles can represent an important issue regarding the development of three dimensional ordering through the formation of large crystallites [23]. The lower spherule size of CB carbon can limit in more extent the reorganization of crystallites than in the case of CBPE2600. CBMeso showed similar XRD profile than CB2800 with almost equal values of the crystallographic parameters. With the exception of graphites, the CNF showed the highest structural ordering according to the values of Table 3.

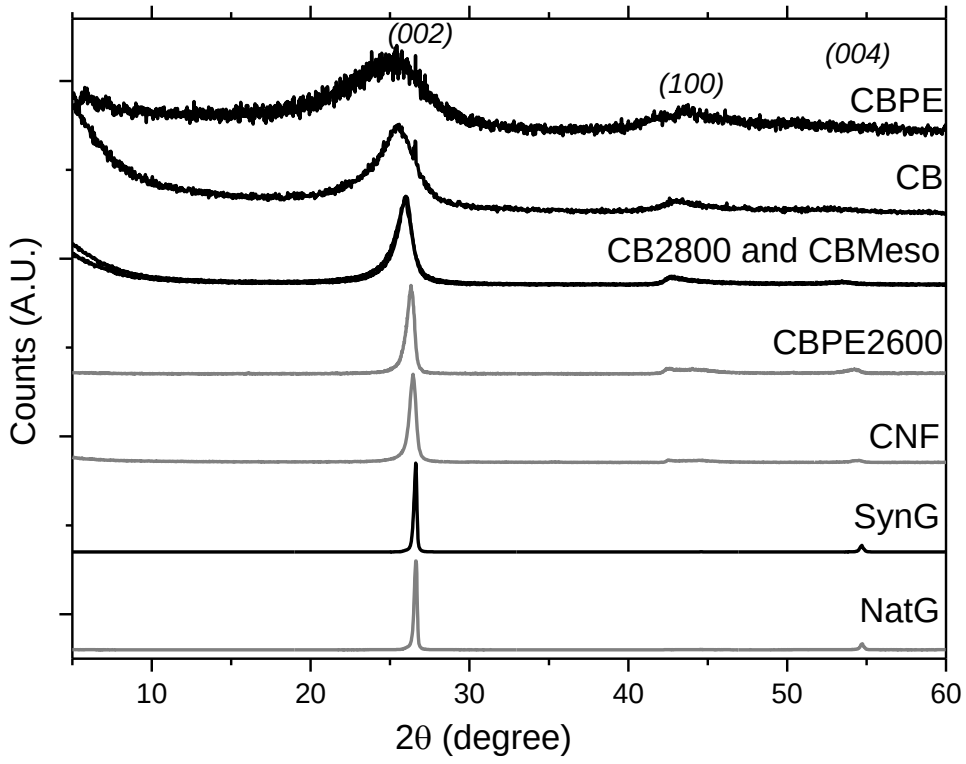

Figure 2. XRD profiles of the carbon supports.

Table 3. Interplanar spacing (d_{002}), crystallite dimensions (L_c and L_a) and I_D/I_G values of the carbon supports.

Support	d_{002} (Å)	L_c (Å)	L_a (Å)	I_D/I_G
CB	3.49	31.9	100.6	1.12
CB2800	3.42	75.0	113.8	0.45
CBPE	3.50	20.4	29.1	0.81
CBPE2600	3.38	135.4	210.4	0.25
NatG	3.35	384.9	798.8	0.00
SynG	3.35	407.6	738.0	0.13
CNF	3.37	176.6	708.4	-
CBMeso	3.42	75.7	136.1	-

Figure 3 shows the RAMAN spectra of selected carbons. The E2g band (≈ 1580 cm^{-1}) was more intense and sharper for SynG and NatG, whereas the band in the 1530 cm^{-1} region, characteristic of turbostratic carbon, was barely detected. The ratio between the intensity of both bands (I_D/I_G) can be used to assess the degree of graphitization. The lower this value, the more developed graphitic structure. Samples CBPE and CB showed the lowest structural order, but after the heat treatment at high temperature it was dramatically improved, especially in the case of CBPE2600.

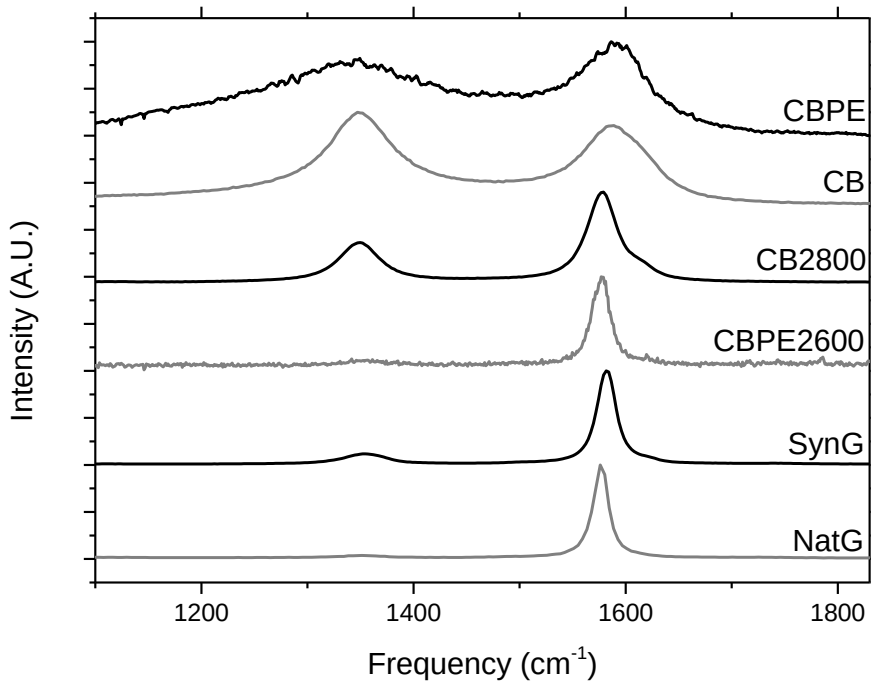

Figure 3. RAMAN spectra for selected carbon supports.

3.2 Characterization of the catalysts

3.2.1 STEM characterization

Table 4 shows the mean diameter of Pd NPs and their corresponding size distribution based on standard deviation. Figure 4 shows typical STEM images and Pd NPs size distributions histograms for the catalysts prepared. By comparing the mean size and size distribution values for Pd/CB2800 (3 and 1 nm, respectively) and Pd/CBPE2600 (9 and 5 nm, respectively) with the ones for Pd/CB (3 and 2 nm, respectively) and Pd/CBPE (11 and 6 nm, respectively), it can be inferred that graphitization of the support does not affect significantly to the size of the Pd NPs on the support. However, the type of starting carbon seems to have a clear influence on the final Pd NPs mean size and size distribution, since a wide range of Pd NPs mean size (3 - 132 nm) and size

distributions (1 – 104 nm) was obtained. The catalysts prepared with a commercial carbon black (Pd/CBMeso) showed the lowest NPs size and shorter size distribution (2 nm and 1 nm, respectively) even lower than for Pd/CB2800 (3 nm and 2 nm, respectively). The catalysts prepared using CNF as support showed a relatively small NP size (4 nm) and size distribution (2 nm). As shown in Figure 4, most of the NPs showed polyhedral-like or pseudo-spherical shapes with the exception of Pd/SynG catalysts which showed mostly irregularly-shaped Pd NPs, probably due to sintering. Some rod-like NPs can also be found in Pd/CBPE2600, Pd/SynG and Pd/NatG catalysts.

Table 4. Size of Pd NPs in the catalysts prepared, Pd^{n+}/Pd^{0} ratio and activity in the aqueous phase HDC of 4-CP.

Catalyst	d_s (nm)	σ_s (nm)	Activity (mmol/g_{Pd}·min)	Pd^{n+}/Pd^{0} initial ratio	Pd^{n+}/Pd^{0} after use ratio
Pd/CB	3	2	63.7	2.0	1.4
Pd/CB2800	3	1	173.5	0.9	0.4
Pd/CBPE	11	6	0.4	1.6	0.6
Pd/CBPE2600	9	5	13.4	1.2	0.3
Pd/NatG	132	104	10.7	1.9	-
Pd/SynG	19	15	36.5	0.5	-
Pd/CBMeso	2	1	138.2	0.6	0.3
Pd/CNF	4	2	96.5	0.4	0.2

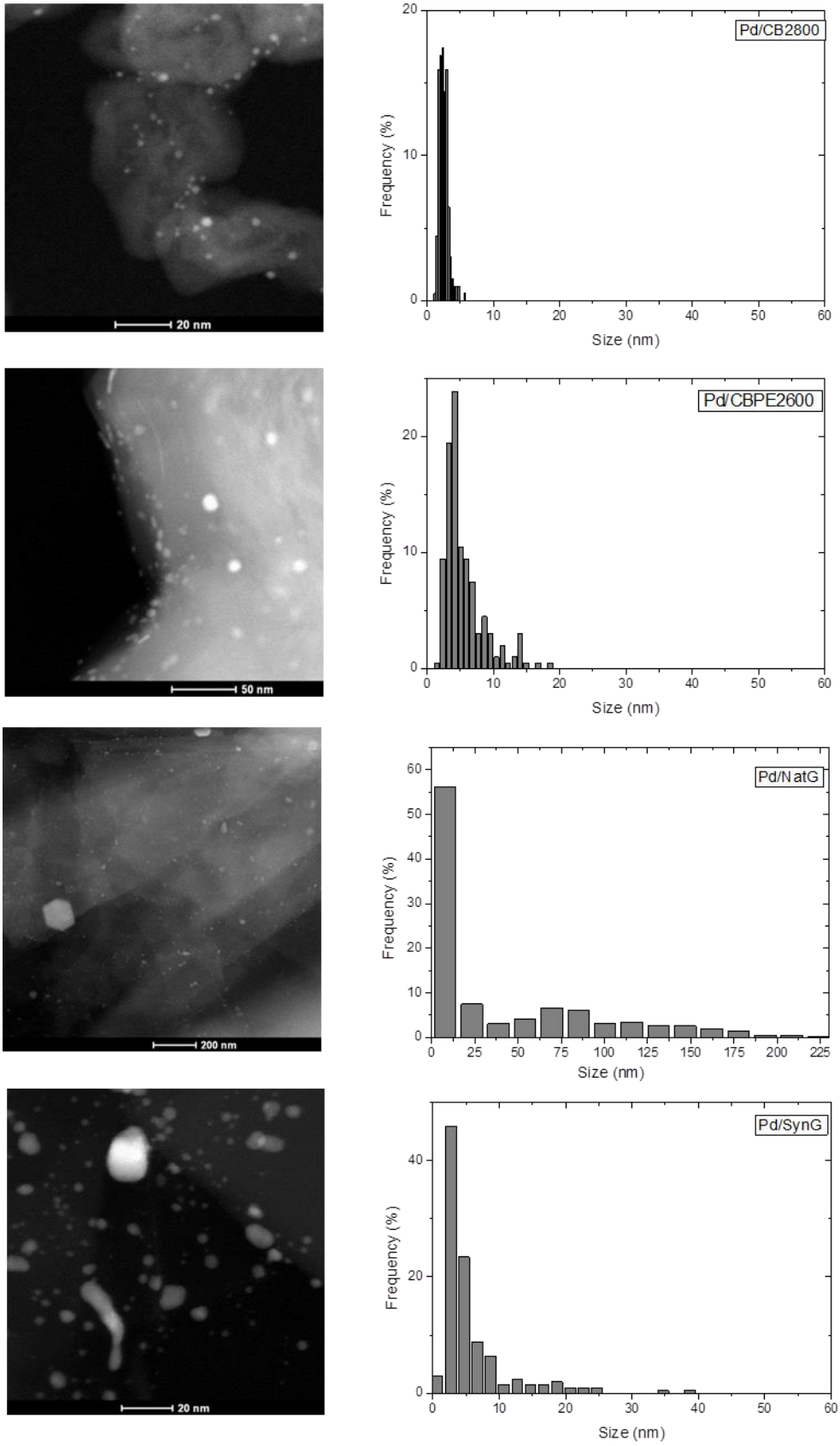

Figure 4. STEM images and size distributions of some of the catalysts prepared

3.2.2 XPS characterization

Figure 5 shows the XPS profiles for the fresh Pd/CB, Pd/CB2800, Pd/CBPE and Pd/CBPE2600 catalysts. The values calculated for the Pd^{n+}/Pd^{0} ratios can be seen in Table 4. Both Pd^{n+} and Pd^{0} species were present in all the cases. All the Pd^{n+}/Pd^{0} values were in a range between 0.4 and 2 for the fresh catalysts, lowering in all cases after their use in HDC (0.2 – 1.4). This must be due to an additional Pd reduction by the H_2 used in the reaction. On the other hand, the Pd^{n+}/Pd^{0} ratio was significantly lower in those catalysts whose support was graphitized upon heat treatment. This could be probably ascribed to the higher electron mobility in graphitized supports towards the active phase, allowing Pd to be reduced in higher extent during the final stage of preparation (reduction under H_2). Consistent with this is the lowest values of Pd/SynG and Pd/CNF catalysts were the lowest. Nevertheless, Pd/NatG showed a comparatively high Pd^{n+}/Pd^{0} ratio which could be related to the higher S content of this graphite support and the possible formation of Pd-sulphur species. When Pd/CBMeso was compared to Pd/CB2800, differences in Pd^{n+}/Pd^{0} ratio were observed, being higher the contribution of Pd^{0} in Pd/CBMeso.

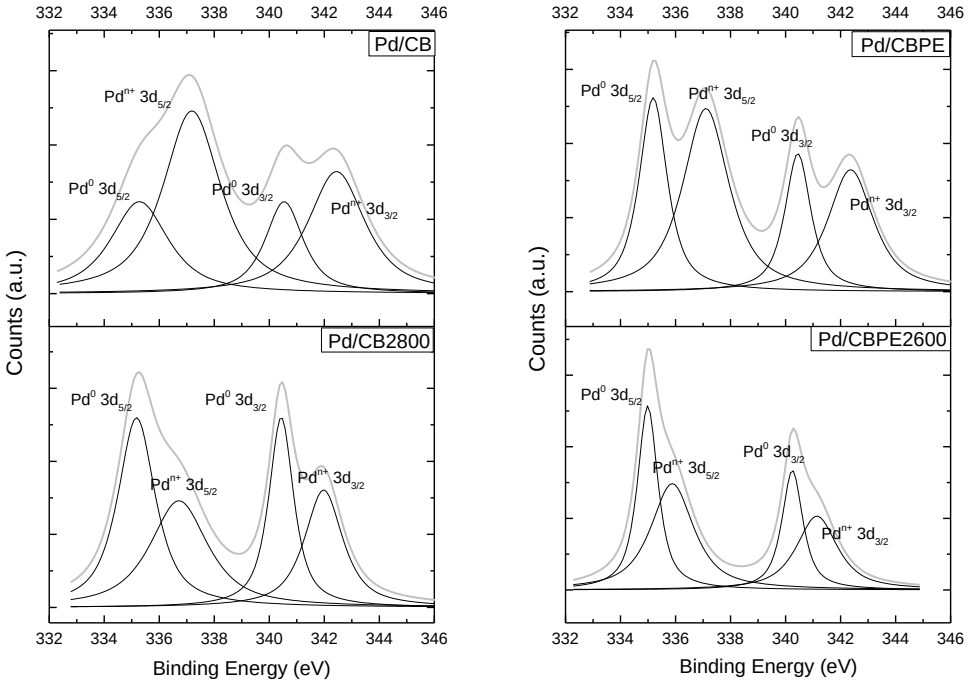

Figure 5. XPS profiles of Pd catalysts using virgin and heat-treated carbon supports

3.3 HDC experiments

3.3.1 Catalysts activity

Preliminary experiments were carried out with all the carbon materials used as supports to check the possible adsorption of 4-CP. It was almost negligible in all the cases (≈ 1 %), in good agreement with the relative low surface areas (< 100 $m^2 \cdot g^{-1}$), with the exception of Pd/CBMeso and Pd/CNF which adsorbed, respectively, 6 % and 4 % of the initial amount of 4-CP at the starting 100 $mg \cdot L^{-1}$ of the experiments. Also, HDC runs performed with the supports without active phase showed that the graphitized ones yielded very low HDC ability (3 % 4-CP conversion at the most).

Figure 6 depicts the 4-CP conversion versus time curves for all the catalysts tested. All of them yielded high 4-CP conversion values (> 99.5 %) after 4 h reaction, except Pd/CBPE which showed very low activity. However, a wide range of activity values were obtained (see Table 4).

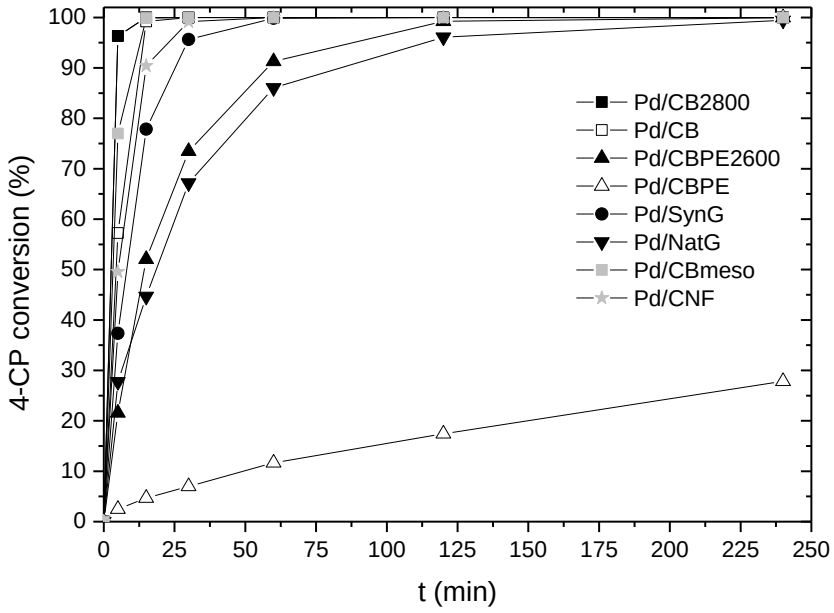

Figure 6. 4-CP conversion versus time curves for the catalysts tested: 30 ºC; 1 atm; $[4\text{-CP}]_0$ = 100 $mg \cdot L^{-1}$; $[Pd]_0$ = 2.5 $mg \cdot L^{-1}$

The catalyst supported on CB2800 showed by far the highest activity, followed by Pd/CBMeso. Pd/CBPE2600 and Pd/NatG yielded the lowest values. Both Pd/CB2800 and Pd/CBMeso showed the highest activity and used equivalent supports (graphitized carbon black), and the small difference in NPs size (3 vs 2 nm) between them could partially explain their different activity. In our previous works, unsupported Rh NPs (2 – 5 nm) were used as model catalysts in the HDC of 4-CP, and a volcano-shaped activity vs NPs size curve was found with the maximum around 2.8 nm [26]. In the case of Pd

the activity was also found to be higher for NPs sized below 3 nm [27]. Kinetic analysis based on the two-step reaction and Langmuir–Hinshelwood mechanisms were applied and the theoretical predictions of the models showed good agreement with the experimental activity data. Decreasing NPs size below the maximum resulted in lower activity due to the higher preference of 4-CP to adsorb on terraces rather than edges and stronger interaction [21]. In this sense, other authors reported that a NPs size range of 3-4 nm was associated to higher catalytic activity of Pd and Rh supported on activated carbon in the HDC of 4-CP [28].

The most active catalysts, Pd/CB2800 and Pd/CBMeso, show also differences in the initial Pd^{n+}/Pd^{0} ratio, being both Pd species more balanced in the former. Some authors have argued that both Pd species in HDC are needed and proposed the dual nature of Pd active sites, being favored the dissociative adsorption of H_2 over Pd^{n+} clusters [29, 30]. They concluded that a balanced contribution of Pd^{n+} and Pd^{0} species, with the ratio around 1, favored the activity in the gas phase HDC of organochlorinated species [29].

The catalysts prepared with the homemade graphitized supports (Pd/CB2800 and Pd/CBPE2600) showed lower and a more balanced initial Pd^{n+}/Pd^{0} ratios (0.9 and 1.2, respectively) than the ones of the catalysts supported on the corresponding CB and CBPE starting carbons (2 and 1.6, respectively). Thus, the more equilibrated contribution of both Pd species in Pd/CB2800 compared to Pd/CB could be associated to the significantly higher activity of the former, in spite of their equivalent mean NPs size (3 nm). In the case of Pd/CBPE2600 and Pd/CBPE, some differences in size (9 vs 11 nm, respectively) and Pd^{n+}/Pd^{0} ratio could also explain their different activity. The reducing ability of the graphitic carbon structures must also be taken into account,

since it can enhance metal–support interactions through electron transfer, favoring hydrogen spillover on the metal–support interface, thus improving the activity [31].

The two catalysts supported on graphites (SynG and NatG) showed some significant differences of activity. This can be mainly explained by the important difference in Pd NPs size (19 and 132 nm, respectively) but it has to be also taken into account the relatively high S content of NatG (0.3 %), which could act as a catalyst poison [32]. Moreover, Pd/SynG showed much lower Pd^{n+}/Pd^{0} ratio, which may be also related with its S content.

The most active catalyst, Pd/CB2800, yielded much higher activity than the reported in previous works for Pd supported on γ-alumina (0.7 $mmol \cdot g_{Pd}^{-1} \cdot min^{-1}$) [33] and Al-pillared clays (0.3 $mmol \cdot g_{Pd}^{-1} \cdot min^{-1}$) [34], Pd supported on nitrogen-doped carbon (55.6 $mmol \cdot g_{Pd}^{-1} \cdot min^{-1}$) [19] and bimetallic RhPd unsupported NPs (67.0 $mmol \cdot g_{Pd}^{-1} \cdot min^{-1}$) [35], but equivalent to the previously obtained with catalysts prepared with CB as support after impregnation with PVP-Pd NPs (ex-situ synthesis) [36].

3.3.2 Catalysts selectivity

In a previous work [37], a reaction scheme was proposed for 4-CP HDC where, in a first step, 4-CP is converted into phenol, which gives rise to cyclohexanone and cyclohexanol upon further hydrogenation. Cyclohexanol also results from cyclohexanone hydrogenation. Direct conversion of 4-CP into cyclohexanone has been also proposed in the literature from kinetic studies [33].

All the catalysts showed only selectivity to phenol or showed only traces of cyclohexanones when 4-CP conversion was less than 100 %. Table 5 shows the selectivity towards phenol, cyclohexanone and cyclohexanol after 4 h of reaction

where except with Pd/CBPE complete 4-CP conversion was achieved. The reduction of Pd during the reaction, as shown by the lower Pd^{n+}/Pd^{0} ratio of the used catalysts (Table 4), could also contribute to increased hydrogenation as the reaction progresses given the higher activity of zerovalent Pd in that respect. However, no significant hydrogenation ability was found for Pd/CBPE2600 and Pd/NatG catalysts, showing selectivity towards phenol higher than 99.9 %. On the contrary, Pd/CB2800, Pd/SynG, Pd/CBMeso and Pd/CNF catalysts showed some selectivity towards cyclohexanone. Cyclohexanol was also found in traces (< 2 mg/L) with the Pd/CB2800, Pd/CBMeso and Pd/CNF catalysts. Comparing the catalysts with and without graphitized support, differences in selectivity were found, especially in the case of the CB-based catalysts with equivalent NPs size. This higher hydrogenation capability could be ascribed to the higher electron density on the catalysts surface, provoked by the charge transferred from the graphitized support to the metal [38]. Other plausible explanation cause could be related with the immobilization of NPs on sites of the graphitized supports that favor the hydrogenation of phenol. In this sense, Wang et al. (2013) reported that Au NPs on the graphitic layers of carbon nanofibers surface were immobilized on their {1 1 1} plane, thus exhibiting more facet area in contrast to the Au NPs supported on less ordered carbon nanofibers surfaces, which were randomly immobilized [39].

Table 5. Selectivity to phenol, cyclohexanone and cyclohexanol of the catalysts synthesized after 4 h reaction.

Sample	Selectivity to		
	phenol (%)	cyclohexanone (%)	cyclohexanol (%)
Pd/CB	92	8	0
Pd/CB2800	86	≈14	t*
Pd/CBPE	100	0	0
Pd/CBPE2600	>99.9	t*	0
Pd/NatG	>99.9	t*	0
Pd/SynG	97	3	0
Pd/CBMeso	88	≈12	t*
Pd/CNF	95	≈5	t*

*Unquantificable traces (< 2 mg / L)

4. Conclusions

Graphitized/graphite carbons with different structural order were used as catalysts supports in the 4-CP aqueous phase. A wide range of Pd NPs mean sizes (3 – 132 nm) and activity values (10.7 – 173.5 mmol·g_{Pd}^{-1}·min^{-1}) were obtained. The most active catalyst (Pd/CB2800, 173.5 mmol·g_{Pd}^{-1}·min^{-1}) showed a Pd NPs mean size of 3 nm and the most balanced contribution of Pd species (initial Pd^{n+}/Pd^0 ratio = 0.9) among the graphitized/graphite supports studied. The effect of the graphitization of the supports on the catalytic activity is clearly observed when the catalysts prepared with a graphitized support (Pd/CB2800 and Pd/CBPE2600, 173.5 and 13.4 mmol·g_{Pd}^{-1}·min^{-1}, respectively) were compared to those with non-graphitized support (Pd/CB and Pd/CBPE, 63.7 and 0.4 mmol·g_{Pd}^{-1}·min^{-1}, respectively) with similar Pd NPs mean size. Increasing the structural order of the support improved the relative amount of zerovalent Pd (Pd^0), leading to a well-balanced contribution of Pd species in the catalysts, which can also be associated to that higher activity. Likewise, higher selectivity to further hydrogenation products (cyclohexanone and cyclohexanol) was obtained with the catalysts supported on graphitized carbons respect to the non-

graphitized ones, especially in the case of the carbon black (CB)-based catalyst (8 % selectivity to cyclohexanone vs 14 % with the catalyst supported in virgin and heat-treated, Pd/CB and Pd/CB2800, respectively).

Acknowledgements

The authors greatly appreciate financial support from the Spanish MINECO (CTQ2012-32821)

References

[1] J. Hagen, Industrial Catalysis: A Practical Approach, 3rd ed., Wiley, New York, 2015.

[2] D.Yu. Murzin, Engineering Catalysis, Walter de Gruyter, Berlin/Boston, 2013.

[3] J.J. Bravo, R.V. Chaudhari, B. Subramaniam, in: Anonymous , American Chemical Society, 2013, pp. 3-68.

[4] B. Machado, P. Serp, Nanostructured Carbon Materials for Catalysis, The Royal Society of Chemistry, 2015, pp. 1-45.

[5] E. Bailón-García, F. J. Maldonado-Hódar, A.F. Pérez-Cadenas, F. Carrasco-Marín, Catalysts. 3 (2013) 853-865.

[6] L. Fang, F.J. Vidal-Iglesias, S.E. Huxter, G.A. Attard, P.B. Wells, Surf. Sci. 631 (2015) 258-266.

[7] S. Bawaked, Q. He, N.F. Dummer, A.F. Carley, D.W. Knight, D. Bethell, C.J. Kiely, G.J., Catal. Sci. Technol. 1 (2011) 747-759.

[8] L. Li, Z.H. Zhu, Z.F. Yan, G.Q. Lu, L. Rintoul, Appl. Catal. A: Gen. 320 (2007) 166-172.

[9] Y. Li, M. Guo, S. Yin, L. Chen, Y. Zhou, R. Qiu, C. Au, Carbon. 55 (2013) 269-275.

[10] M. Hara, M. Lee, C. Liu, B. Chen, Y. Yamashita, M. Uchida, H. Uchida, M. Watanabe, Electrochim. Acta. 70 (2012) 171-181.

[11] H. Yano, T. Akiyama, M. Watanabe, H. Uchida, J. Electroanal. Chem. 688 (2013) 137-142.

[12] S.S. Jeon, W.B. Han, H.H. An, S.S. Im, C.S. Yoon, Appl. Catal. A: Gen. 409–410 (2011) 156-161.

[13] A.G. Ruiz, J.D.L. Gonzalez, I.R. Ramos, J. Chem. Soc. -Chem. Commun. (1984) 1681-1682.

[14] M.A. Keane, ChemCatChem. 3 (2011) 800-821.

[15] C. Amorim, G. Yuan, P.M. Patterson, M.A. Keane, J. Catal. 234 (2005) 268-281.

[16] M.A. Keane, C. Park, C. Menini, Catal. Lett. 88 (2003) 89-94.

[17] E. Díaz, S. Ordóñez, R.F. Bueres, E. Asedegbega-Nieto, H. Sastre, Appl. Catal. B: Environ. 99 (2010) 181-190.

[18] M. Munoz, S. Ponce, G. Zhang, B.J.M. Etzold, Appl. Catal. B: Environ. 192 (2016) 1-7.

[19] J.A. Baeza, N. Alonso-Morales, L. Calvo, F. Heras, J.J. Rodriguez, M.A. Gilarranz, Carbon. 87 (2015) 444-452.

[20] N. Alonso-Morales, M.A. Gilarranz, F. Heras, S. Eser, J.J. Rodriguez, Energy Fuels. 23 (2009) 6095-6101.

[21] J.A. Baeza, L. Calvo, D.Y. Murzin, J.J. Rodriguez, M.A. Gilarranz, Catal. Lett. 144 (2014) 2080-2085.

[22] D.Y. Murzin, J. Catal. 276 (2010) 85-91.

[23] N. Alonso-Morales, M.A. Gilarranz, F. Heras, J.J. Rodriguez, S. Eser, Chem. Eng. J. 172 (2011) 1126-1136.

[24] Z.Q. Li, C.J. Lu, Z.P. Xia, Y. Zhou, Z. Luo, Carbon. 45 (2007) 1686-1695.

[25] A. Marchand, in: Figueiredo, J.L. and Moulijn, J.A. (Eds.), Carbon and Coal Gasification: Science and Technology, Springer Netherlands, Dordrecht, 1986, pp. 93-136.

[26] J.A. Baeza, L. Calvo, M.A. Gilarranz, J.J. Rodriguez, Chem. Eng. J. 240 (2014) 271-280.

[27] J.A. Baeza, L. Calvo, M.A. Gilarranz, A.F. Mohedano, J.A. Casas, J.J. Rodriguez, J. Catal. 293 (2012) 85-93.

[28] E. Diaz, A.F. Mohedano, J.A. Casas, L. Calvo, M.A. Gilarranz, J.J. Rodriguez, Appl. Catal. B: Environ. 106 (2011) 469-475.

[29] L. Gomez-Sainero, X. Seoane, J. Fierro, A. Arcoya, J. Catal. 209 (2002) 279-288.

[30] S. Omar, J. Palomar, L.M. Gomez-Sainero, M.A. Alvarez-Montero, M. Martin-Martinez, J.J. Rodriguez, J. Phys. Chem. C. 115 (2011) 14180-14192.

[31] J. Feng, Y. He, Y. Liu, Y. Du, D. Li, Chem. Soc. Rev. 44 (2015) 5291-5319.

[32] J. Oudar, Catal. Rev.: Sci. Eng. 22 (1980) 171-195.

[33] E. Díaz, J.A. Casas, A.F. Mohedano, L. Calvo, M.A. Gilarranz, J.J. Rodríguez, Ind. Eng. Chem. Res. 47 (2008) 3840-3846.

[34] C.B. Molina, L. Calvo, M.A. Gilarranz, J.A. Casas, J.J. Rodriguez, J. Hazard. Mater. 172 (2009) 214-223.

[35] J.A. Baeza, L. Calvo, J.J. Rodriguez, E. Carbó-Argibay, J. Rivas, M.A. Gilarranz, Appl. Catal. B: Environ. 168–169 (2015) 283-292.

[36] J.A. Baeza, L. Calvo, J.J. Rodriguez, M.A. Gilarranz, Chem. Eng. J. 294 (2016) 40-48.

[37] L. Calvo, A.F. Mohedano, J.A. Casas, M.A. Gilarranz, J.J. Rodríguez, Carbon. 42 (2004) 1377-1381.

[38] A. Giroir-Fendler, D. Richard, P. Gallezot, Stud. Surf. Sci. Catal. 41 (1988) 171-178.

[39] D. Wang, A. Villa, D. Su, L. Prati, R. Schlögl, ChemCatChem. 5 (2013) 2717-2723.